Expanding Photonic Integrated Circuits into the UVC Region: Design, Fabrication, and Perspective of Low Loss SiO_x Waveguides

Chenming Su,[1,2] Chupao Lin,[1,2] Roel Baets[1,2], and Nicolas Le Thomas[1,2]

[1] Photonics Research Group, INTEC Department, Ghent University-imec, Technologiepark-Zwijnaarde, 9052 Ghent, Belgium
[2] Center for Nano- and Biophotonics, Ghent University, Belgium

Abstract

Photonic integrated circuits (PICs) have enabled a large number of applications by using light from the visible to mid-infrared spectrum, but not yet in the ultraviolet-C (UVC, λ = 200 – 280 nm) spectral region. Considering that most of the biomolecules have strong absorption in the UVC, PICs operating in this wavelength range are envisioned to spark new biosensing and biomedical applications. However, the development of PICs in the UVC region is hindered by significant scattering and absorption losses, and limited choices of waveguide materials. Addressing these hurdles, we propose a suspended waveguide design with air-cladding on a silicon substrate. The core of the waveguide is made of thermal silicon oxide. Simulations and optimizations were conducted to identify a single-mode regime at λ = 266 nm. The waveguides were fabricated with a two-step electron beam lithography patterning process. As a result, we achieved propagation losses of 5 dB/cm for single-mode waveguides and 2.4 dB/cm for multi-mode waveguides at λ = 266 nm. Furthermore, we delved into the limiting factors of propagation losses in the UVC region. This work demonstrates on-chip low-loss waveguides in the UVC range and paves the way for on-chip UVC resonance Raman spectroscopy.

Introduction

Photonic Integrated Circuits (PICs) are revolutionizing a large number of technological areas including bioscience [1], super-resolution microscopy [2], and artificial intelligence [3] due to their compactness and cost-effectiveness for large-scale fabrication. Most current PICs operate in the visible to mid-infrared wavelength range, leaving the ultraviolet (UV) region, in particular the UVC subset, barely explored until now. However, the UVC range has unique properties in terms of light-matter interaction, which makes it promising for biosensing, pharmaceutical research, and environmental monitoring. For instance, UVC light is strongly absorbed by many biomolecules, which is crucial for techniques like absorption spectroscopy, Raman sensing, and auto-fluorescence microscopy.

To develop a PIC platform in the UVC region, the fundamental building block is the waveguide: it has to propagate a single mode of light with losses at least lower than 5dB/cm and be compatible with the complementary metal-oxide-semiconductor (CMOS) technology. In this paper, we propose and optimize by simulations a silica waveguide design at an operating wavelength λ = 266 nm. After discussing the fabrication steps of such a waveguide design, we focus on the experimental propagation loss.

Design and simulation

Only a limited number of materials have high transmission in the UV region, such as high-purity silica, calcium fluoride (CaF_2), alumina (AlO_x), and silicon oxynitride (SiON).

Although AlO_x PICs have been shown to be compatible with the UVA wavelength range (320 – 400 nm) [2], they currently exhibits high propagation losses in the UVC. On the other hand, it has been reported that SiON channel waveguides achieve propagation losses as low as 1 dB/cm in the UVC region [4]. However, such waveguides are defined by extremely low refractive index contrast (Δn=0.023) between the core and cladding, which is inconvenient for waveguide based sensing applications. High-purity silica and CaF_2 are difficult to obtain on silicon substrate. Considering these constrains, we focus on thermally grown SiO_x layer with the hypothesis that it may have excellent UVC transmission properties while being compatible with the standard CMOS fabrication process.

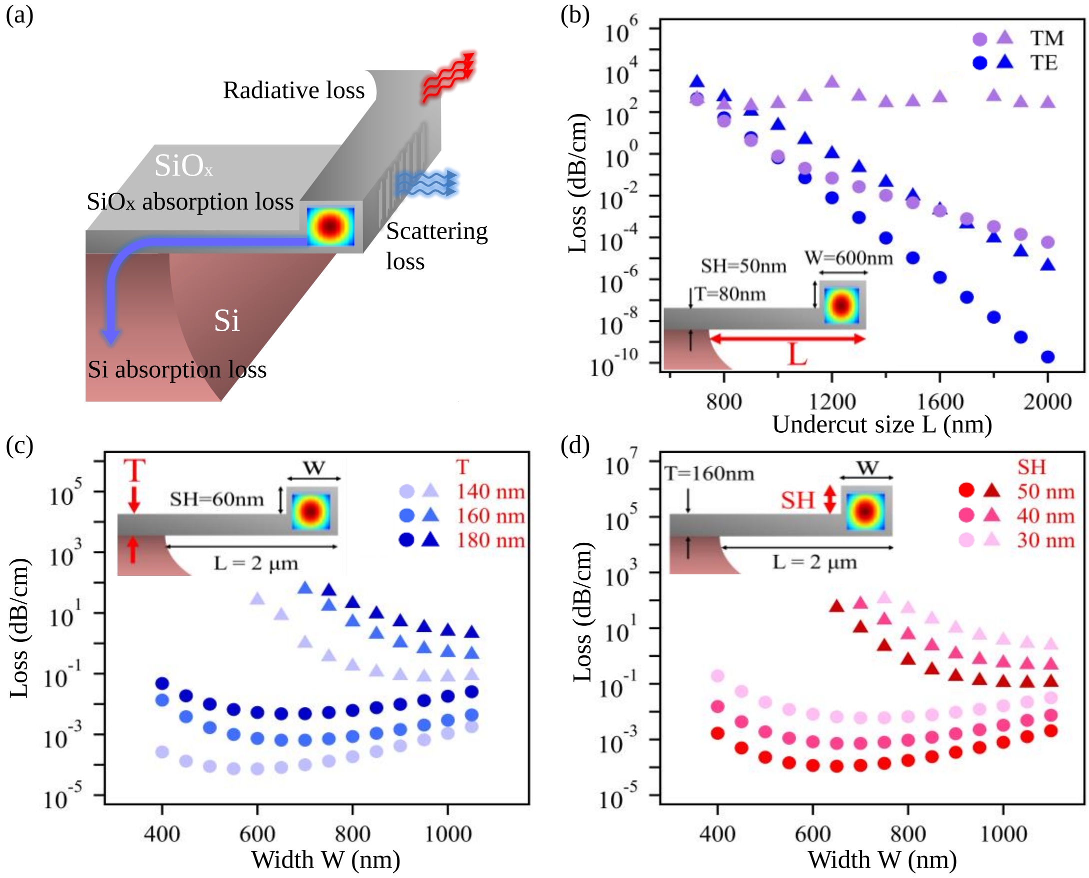

Figure 1: (a) Schematic of the design of a suspended SiO_x waveguide and the origins of losses; (b), (c), and (d) indicate the simulated loss at λ = 266 nm with respect to L, SH, and T for various waveguide widths W, respectively. The solid circles and triangles represent the fundamental modes and the first higher-order modes respectively.

To minimize the significant absorption loss of the silicon substrate in the UV region, we designed the waveguide on a free-standing SiO_x layer with air cladding, which requires etching away the silicon substrate underneath. The structure of the waveguide that is defined at the edge of the under etch SiO_x membrane is schematically represented in Fig. 1(a). As indicated in this figure, four main sources of losses are expected: 1) absorption loss from the silicon substrate that can be decreased by increasing the size L of the undercut, 2) the intrinsic SiO_x absorption loss that is expected to be low in view of the loss performances of optical fibers in the UV, 3) radiative losses at the bends and 4) Scattering losses from the sidewalls that become more pronounced at shorter wavelengths ($\sim \lambda^{-4}$). A relatively large bending radius, for example, 200 µm, contributes to reduce the radiative loss at the bends. Scattering losses can be minimized either by decreasing the sidewall roughness with an optimized etching process or by increasing the waveguide width to decrease the field amplitude of the propagating mode at the sidewalls.

Four parameters of the design are critical to achieve a single-mode waveguide with low loss at λ = 266 nm: the SiO_x step height (SH), the SiO_x layer thickness (T), the SiO_x waveguide width (W), and the undercut size (L). We have explored the corresponding parameter space to track the optimal geometry by simulating the propagation losses with the MODE solver in the Lumerical software. The relationship between loss and L is presented in Fig. 1(b) with a preliminary setting for the other three parameters T, W, and SH. Loss decreases for larger values of L, reaching for the fundamental TE mode 10^{-9} dB/cm for L=2 µm. Beyond L=2 µm, buckling or wrinkle of the membrane are expected to take place. Figure 1(c) illustrates that a smaller thickness T reduces losses by limiting the light leakage to the silicon. However, as the width-boundary for a single-mode waveguide also shrinks with a smaller T, the thickness should not be excessively small to minimize the scattering losses at the sidewalls. Moreover, the intrinsic stress in the SiO_x layer leads to the buckling of the membrane when T is too small. To maintain structural stability and low loss, T should be larger than 160 nm for an undercut size L of 2 µm. Figure 1(d) reveals that the losses of both the fundamental and the first higher-order TE modes drops as the step height increases. This is accompanied with a concomitant decrease of the optimal waveguide width W, which contributes to enhance the impact of the sidewalls roughness. Finally, our simulations suggest that an optimal set of parameters is L=2 µm, T=160 nm, SH=40 nm and W=650 nm, for which losses as low as 10^{-3} dB/cm are predicted. We discuss below the actual experimental losses of a waveguide designed with such parameters.

Fabrication

The waveguides are patterned by a two-step electron beam lithography (EBL) and etched by an inductively coupled plasma - reactive ion etching (ICP-RIE) tool. Utilizing four-inch wafers with 300 nm thermally oxidized SiO_x on silicon substrate, the first EBL patterning and anisotropic ICP-RIE etching (indicated by the red arrow) generate a 3-µm-wide trench, while the second EBL step is used to produce a shallow etch that defines the waveguide profile (indicated by the yellow arrow), as depicted in Figure 2(a). Then the whole structure is etched down to ensure an appropriate SiO_x layer thickness after the isotropic etching of silicon (indicated by the violet arrow). The etching recipes have been fine-tuned to produce a smooth sidewall. A scanning electron microscope (SEM) image of a typical waveguide is shown in Figure 2(b), validating the fabrication process. It is worth noting that this two-step EBL patterning method introduces an overlay error in the waveguide width, which generates extra losses.

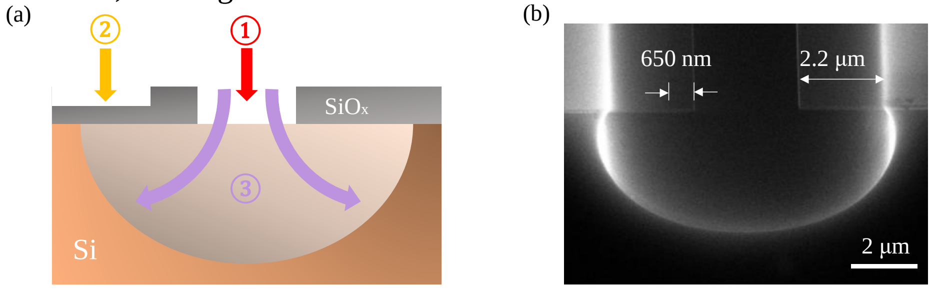

Figure 2: (a) Fabrication process of the suspended waveguide; (b) SEM image of a 650 nm wide suspended waveguide.

Loss Measurement

UVC light from a pulsed laser (λ = 266 nm) is edge-coupled into the waveguides. Figure 3(a) shows the image of the scattered UVC light from the top surface of one of the processed spiral waveguides: the light intensity decays along the propagation in the spiral. After several turns, weak UVC light still propagates out of the spiral as the purple arrow indicates. Mean pixel values are extracted from six regions (indicated by the yellow dashed lines) on the spiral for loss measurement, which defines the error bars in Figure 3(b). Ultimately, the relationship between losses and various waveguide widths is depicted in Figure 3(b). With the high index contrast (Δn~0.5), we achieved losses of 5 dB/cm for a single-mode waveguide and an even lower value of 2.4 dB/cm for a multi-mode waveguide.

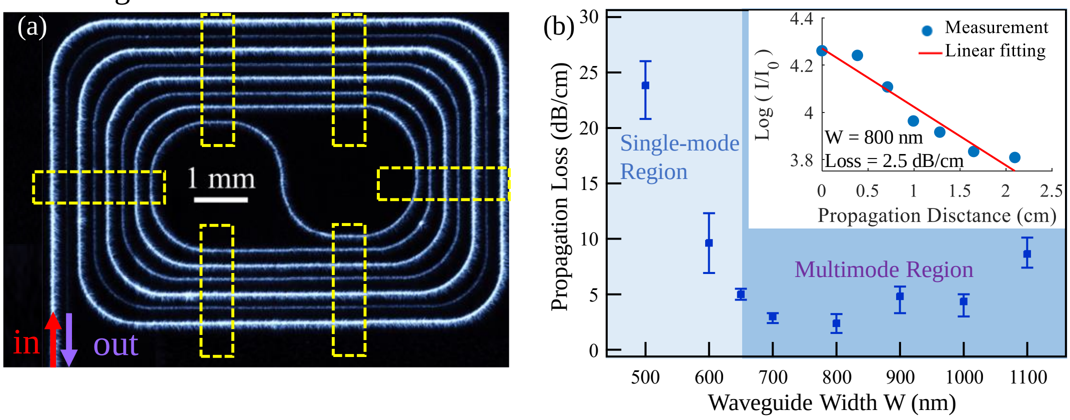

Figure 3: (a) Image of the scattered light from a spiral waveguide at λ=266 nm. (b) Loss extraction from the decay of light intensity and propagation length, as well as the relationship between the propagation loss and waveguide width. I is the intensity after a certain propagation distance and I_0 is the original intensity.

Conclusions

We have investigated a suspended SiO_x waveguide for UVC applications. We reached loss values already relevant for simple designs of PICs: 2.4 dB/cm for multi-mode waveguides and 5 dB/cm for single-mode waveguides. We suspect that the losses are not yet limited by the intrinsic absorption losses of the thermal silicon oxide. The scattering loss could be further diminished by optimizing the etching recipes. Dedicated designed bends, such as partial Euler bends, could help to further minimize the radiative loss. Also, a new patterning approach in the two step EBL process might accommodate the overlay error leading to even lower losses. This will pave the way for sophisticated PICs in the UVC domain, facilitating applications like on-chip UV Raman sensing while preserving CMOS compatibility.

References

[1] Z. Liu *et al.*, "Ultra-sensitive slot-waveguide-enhanced Raman spectroscopy for aqueous solutions of non-polar compounds using a functionalized silicon nitride photonic integrated circuit," *Opt. Lett.*, vol. 46, no. 5, pp. 1153–1156, Mar. 2021, doi: 10.1364/OL.416464.
[2] C. Lin *et al.*, "UV photonic integrated circuits for far-field structured illumination autofluorescence microscopy," *Nat. Commun.*, vol. 13, no. 1, Art. no. 1, Jul. 2022, doi: 10.1038/s41467-022-31989-8.
[3] Y. Shen *et al.*, "Deep Learning with Coherent Nanophotonic Circuits," *Nat. Photonics*, vol. 11, no. 7, pp. 441–446, Jul. 2017, doi: 10.1038/nphoton.2017.93.
[4] K. B. Mogensen *et al.*, "Ultraviolet transparent silicon oxynitride waveguides for biochemical microsystems," *Opt. Lett.*, vol. 26, no. 10, pp. 716–718, May 2001, doi: 10.1364/OL.26.000716.